Exchange interaction in the yellow exciton series of cuprous oxide

Patric Rommel [*] and Jörg Main
Institut für Theoretische Physik 1, Universität Stuttgart, 70550 Stuttgart, Germany

Andreas Farenbruch [1] Dmitri R. Yakovlev [1,2] and Manfred Bayer [1,2]
[1]*Experimentelle Physik 2, Technische Universität Dortmund, 44221 Dortmund, Germany*
[2]*Ioffe Institute, Russian Academy of Sciences, 194021 St. Petersburg, Russia*

(Received 12 November 2020; accepted 5 February 2021; published 18 February 2021)

We experimentally and numerically investigate the exchange interaction of the yellow excitons in cuprous oxide. By varying the material parameters in the numerical calculations, we can interpret experimental findings and understand their origin in the complex band structure and central-cell corrections. In particular, we experimentally observe the reversal of the ortho- and paraexciton for the 2*S* yellow exciton and explain this phenomenon by an avoided crossing with the green 1*S* orthoexciton in a detailed numerical analysis. Furthermore, we discuss the exchange splitting as a function of the principal quantum number n and its deviation from the n^{-3} behavior expected from a hydrogenlike model. We also explain why the observed exchange splitting of the green 1*S* exciton is more than twice the splitting of the yellow 1*S* state.

DOI: 10.1103/PhysRevB.103.075202

I. INTRODUCTION

The yellow exciton series in cuprous oxide has been shown to closely match a hydrogenlike system in many respects [1]. Still, there are a number of characteristic effects of the complex band structure. For example, a fine-structure splitting between P and F states can be observed [2]. In the case of small radii, additional central-cell corrections to the valence band Hamiltonian have to be added to achieve a satisfactory description [3]. Due to the cubic symmetry of the crystal, the angular momentum is not a good quantum number anymore, and thus, the S states with small extension are also coupled to other angular momenta, such as the D states. This is especially important when considering the green 1*S* state, which lies in between the yellow spectrum. Because of this coupling, the central-cell corrections also affect the energetically higher-lying states of the yellow series.

The exchange interaction, which is part of the central-cell corrections, causes a characteristic splitting between states depending on the relative alignment of the electron and hole spins, i.e., between the spin-singlet and spin-triplet states. The spin-triplet dark exciton states have been proposed for use in quantum computational applications and for the possible realization of a Bose-Einstein condensate [4–6]. The dark paraexciton series in cuprous oxide is not accessible by electric dipole and quadrupole absorption experiments because the paraexcitons have no spin-singlet component and are therefore spin flip forbidden to all orders in electric transitions. This selection rule can be circumvented using stress [7] or by application of an external magnetic field which leads to a mixing between spin-singlet and -triplet states [8,9]. We use magnetic-field-induced second-harmonic generation (SHG) spectroscopy for the measurements of the paraexcitons, extrapolating their magnetic-field-dependent energies to zero field strength.

A naive treatment of the exchange interaction leads to the expectation that the orthoexciton is shifted to higher energies than the paraexciton, a result in line with Hund's rule. Numerical calculations have shown that this expectation is contradicted in the case of the yellow 2*S* exciton state in cuprous oxide [3]. This has now been confirmed in experiments by Farenbruch *et al.* [10]. They explain this by appealing to the influence of the green 1*S* state. In this paper, we discuss and confirm this explanation in greater detail, using the possibility of changing the material parameters in the numerical simulations to study the spectrum in experimentally inaccessible ways. Going beyond the discussion in Ref. [10], we present the precise mechanism responsible for the reversed energies of the 2*S* ortho- and paraexcitons. We then study the exchange splitting as a function of the principal quantum number n. Based on a hydrogenlike calculation, the splitting is expected to decrease with n^{-3}. For the yellow excitons in cuprous oxide, there are deviations from this. We numerically investigate the origin of these deviations. We also explain why the exchange splitting of the green 1*S* state is more than twice the exchange splitting of the yellow 1*S* state. To the best of our knowledge, this represents the first detailed discussion of these features of the dark exciton series in cuprous oxide.

This paper is organized as follows: We first introduce the Hamiltonian and focus on the central-cell corrections

[*]patric.rommel@itp1.uni-stuttgart.de

in Sec. II A. We briefly explain our numerical methods in Sec. II B and our experimental methods in Sec. II C. In Sec. III, we discuss the reversal between the 2*S* ortho- and paraexcitons (Sec. III A), the exchange splitting as a function of the principal quantum number (Sec. III B), and the splitting of the yellow 1*S* state versus the green 1*S* state (Sec. III C). We finally conclude in Sec. IV.

II. METHODS AND MATERIALS

In this section, we introduce the theoretical background for the description of the yellow exciton series and our method of numerical diagonalization. Furthermore, we explain our experimental methods.

A. Hamiltonian including central-cell corrections

Excitons are described as hydrogenlike excitations of the crystal, where an electron is lifted from one of the valence bands to the conduction band, leaving behind a hole. The complex valence band structure can be described via a quasispin $\boldsymbol{I}$ in addition to the hole spin $\boldsymbol{S}_\mathrm{h}$. This description introduces additional degrees of freedom compared to the hydrogenlike model. For a detailed analysis, especially of the ortho and para 2*S* states, central-cell corrections are required. Details of the derivations were already presented in the literature [3,11–15]. For the convenience of the reader in this paper we briefly recapitulate the basic equations.

The yellow and green exciton series in cuprous oxide (Cu_2O) belong to the Γ_7^+ and Γ_8^+ valence bands, respectively. They can be described using the Hamiltonian [11]

$$H = E_\mathrm{g} + H_\mathrm{e}(\boldsymbol{p}_\mathrm{e}) + H_\mathrm{h}(\boldsymbol{p}_\mathrm{h}) + V(\boldsymbol{r}_\mathrm{e} - \boldsymbol{r}_\mathrm{h}) + V_\mathrm{CCC}^\mathrm{H}(\boldsymbol{r}). \quad (1)$$

Here E_g is the band gap between the uppermost Γ_7^+ valence band and the lowermost Γ_6^+ conduction band. The kinetic energies of the electron and hole are given by

$$H_\mathrm{e}(\boldsymbol{p}_\mathrm{e}) = \frac{\boldsymbol{p}_\mathrm{e}^2}{2m_\mathrm{e}}, \quad (2)$$

$$\begin{aligned} H_\mathrm{h}(\boldsymbol{p}_\mathrm{h}) = {} & H_\mathrm{SO} + \frac{1}{2\hbar^2 m_0}\big[\hbar^2(\gamma_1 + 4\gamma_2)\boldsymbol{p}_\mathrm{h}^2 \\ & + 2(\eta_1 + 2\eta_2)\boldsymbol{p}_\mathrm{h}^2(\boldsymbol{I}\cdot\boldsymbol{S}_\mathrm{h}) \\ & - 6\gamma_2\big(p_{\mathrm{h}1}^2 \boldsymbol{I}_1^2 + \mathrm{c.p.}\big) - 12\eta_2\big(p_{\mathrm{h}1}^2 \boldsymbol{I}_1 \boldsymbol{S}_{\mathrm{h}1} + \mathrm{c.p.}\big) \\ & - 12\gamma_3(\{p_{\mathrm{h}1}, p_{\mathrm{h}2}\}\{\boldsymbol{I}_1, \boldsymbol{I}_2\} + \mathrm{c.p.}) \\ & - 12\eta_3(\{p_{\mathrm{h}1}, p_{\mathrm{h}2}\}(\boldsymbol{I}_1\boldsymbol{S}_{\mathrm{h}2} + \boldsymbol{I}_2\boldsymbol{S}_{\mathrm{h}1}) + \mathrm{c.p.})\big]. \end{aligned} \quad (3)$$

We use the electron mass in the crystal m_e and in vacuum m_0, the Luttinger parameters γ_i and η_i, the spin $\boldsymbol{S}_\mathrm{h}$ and quasispin $\boldsymbol{I}_i$ of the hole, and the momenta $\boldsymbol{p}_\mathrm{e}$ and $\boldsymbol{p}_\mathrm{h}$ of the electron and hole, respectively. The indices $i = 1, 2, 3$ for the momenta, positions, quasispin, and hole spin denote the Cartesian x, y, and z components; c.p. denotes cyclic permutation. The spin-orbit coupling term reads

$$H_\mathrm{SO} = \frac{2}{3}\Delta\left(1 + \frac{1}{\hbar^2}\boldsymbol{I}\cdot\boldsymbol{S}_\mathrm{h}\right). \quad (4)$$

The electron and hole interact via the screened Coulomb potential

$$V(\boldsymbol{r}_\mathrm{e} - \boldsymbol{r}_\mathrm{h}) = -\frac{e^2}{4\pi\varepsilon_0\varepsilon|\boldsymbol{r}_\mathrm{e} - \boldsymbol{r}_\mathrm{h}|}, \quad (5)$$

with the dielectric constant $\varepsilon = \varepsilon_{\mathrm{s}1}$ and the positions of the electron $\boldsymbol{r}_\mathrm{e}$ and hole $\boldsymbol{r}_\mathrm{h}$. We express the system in relative and center-of-mass coordinates [16],

$$\begin{aligned} \boldsymbol{r} &= \boldsymbol{r}_\mathrm{e} - \boldsymbol{r}_\mathrm{h}, \quad \boldsymbol{R} = \frac{m_\mathrm{h}\boldsymbol{r}_\mathrm{h} + m_\mathrm{e}\boldsymbol{r}_\mathrm{e}}{m_\mathrm{h} + m_\mathrm{e}}, \\ \boldsymbol{P} &= \boldsymbol{p}_\mathrm{e} + \boldsymbol{p}_\mathrm{h}, \quad \boldsymbol{p} = \frac{m_\mathrm{h}\boldsymbol{p}_\mathrm{e} - m_\mathrm{e}\boldsymbol{p}_\mathrm{h}}{m_\mathrm{h} + m_\mathrm{e}}, \end{aligned} \quad (6)$$

with vanishing center-of-mass momentum $\boldsymbol{P} = 0$.

For small separations, the electron-hole pair probes features of the crystal structure not captured by the valence band terms given in Eq. (3). Furthermore, the dielectric constant ε in Eq. (5) is no longer constant. The corresponding corrections to the Hamiltonian are the central-cell corrections [12–15], and they primarily concern the states with principal quantum number $n \leqslant 2$. As derived in Ref. [3], the central-cell corrections in cuprous oxide are given by

$$V_\mathrm{CCC}^\mathrm{H}(\boldsymbol{r}) = V^\mathrm{H} + H_\mathrm{exch} + V_d, \quad (7)$$

where

$$\begin{aligned} V^\mathrm{H} = {} & -\frac{e^2}{4\pi\varepsilon_0 r}\left[\frac{1}{2\varepsilon_1^*}(e^{-r/\rho_{\mathrm{h}1}} + e^{-r/\rho_{\mathrm{e}1}})\right. \\ & \left. + \frac{1}{2\varepsilon_2^*}(e^{-r/\rho_{\mathrm{h}2}} + e^{-r/\rho_{\mathrm{e}2}})\right] \end{aligned} \quad (8)$$

is the Haken potential describing the modification of the dielectric constant for electron-hole separations on the order of the polaron radii, with further corrections modeled by a contact interaction

$$V_d = -V_0 V_\mathrm{uc}\delta(\boldsymbol{r}), \quad (9)$$

with the volume of a lattice unit cell $V_\mathrm{uc} = a^3$ and the lattice constant a. We use

$$\frac{1}{\varepsilon_i^*} = \frac{1}{\varepsilon_{\mathrm{b}i}} - \frac{1}{\varepsilon_{\mathrm{s}i}} \quad (10)$$

and the polaron radii

$$\rho_{\mathrm{e}i} = \sqrt{\frac{\hbar}{2m_\mathrm{e}\omega_{\mathrm{LO}i}}}, \qquad \rho_{\mathrm{h}i} = \sqrt{\frac{\hbar\gamma_1}{2m_0\omega_{\mathrm{LO}i}}}, \quad (11)$$

with the energies $\hbar\omega_{\mathrm{LO}i}$ of the longitudinal Γ_4^- phonons. The relevant phonon branches are marked with $i = 1, 2$. The exchange interaction is given in Ref. [3] and reads

$$\begin{aligned} H_\mathrm{exch} &= J_0\left(\frac{1}{4} - \frac{1}{\hbar^2}\boldsymbol{S}_\mathrm{e}\cdot\boldsymbol{S}_\mathrm{h}\right)V_\mathrm{uc}\delta(\boldsymbol{r}) \\ &= J_0\left(1 - \frac{1}{2\hbar^2}\boldsymbol{S}^2\right)V_\mathrm{uc}\delta(\boldsymbol{r}), \end{aligned} \quad (12)$$

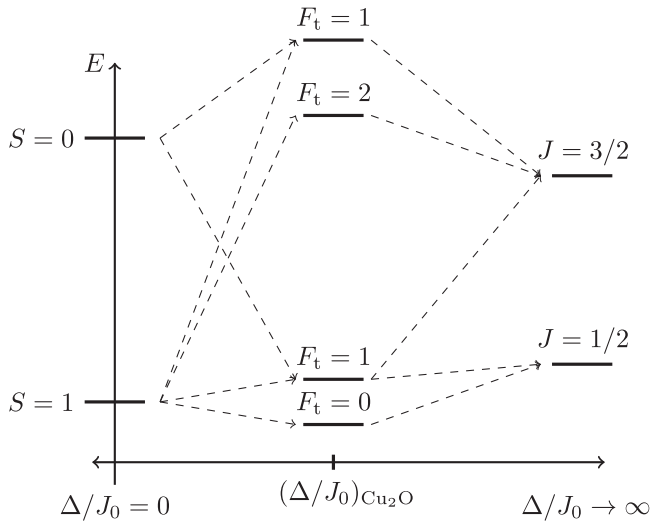

FIG. 1. Level scheme of S states as a function of the ratio between the exchange interaction strength J_0 and the spin-orbit coupling Δ. For $L = 0$, the total angular momentum F_t can be obtained by either coupling the quasispin of the hole $\boldsymbol{I}$ with the total spin $\boldsymbol{S} = \boldsymbol{S}_e + \boldsymbol{S}_h$ or by coupling the electron spin $\boldsymbol{S}_e$ with the effective hole spin $\boldsymbol{J} = \boldsymbol{I} + \boldsymbol{S}_h$. According to Eq. (12), the $S = 0$ singlet states are lifted above the $S = 1$ triplet states for vanishing spin-orbit coupling Δ. For $\Delta/J_0 \to \infty$, the splitting between the green $J = 3/2$ and yellow $J = 1/2$ states predominates. For general values in between, the levels split according to the total angular momentum F_t. As discussed in Sec. III C with reference to the matrix element (16), for both the green and yellow S states, the $F_t = 1$ states are lifted above the $F_t = 2$ and $F_t = 0$ states, respectively.

where we use the total spin $\boldsymbol{S} = \boldsymbol{S}_e + \boldsymbol{S}_h$ in the second part of the equation. We want to take a closer look at the exchange interaction (12) in the following.

We first note that only $L = 0$ states are affected due to the presence of the δ term. From the second line in Eq. (12) it is clear that the effect is a lifting of the states with $S = 0$ over the states with $S = 1$. When taking into account the quasispin $\boldsymbol{I}$ in the crystal, S is not a good quantum number anymore, and we additionally need to consider the spin-orbit coupling given in Eq. (4). In Fig. 1 we show the level scheme of the S states caused by the competition between the exchange interaction and the spin-orbit coupling as a function of the ratio Δ/J_0. Note that for the yellow $J = 1/2$ states only the threefold-degenerate $F_t = 1$ orthoexcitons have an $S = 0$ component and are therefore dipole allowed. Here $\boldsymbol{F}_t = \boldsymbol{J} + \boldsymbol{S}_e = \boldsymbol{I} + \boldsymbol{S}$ is the total angular momentum. While the singlet state $S = 0$ is lifted above the triplet state $S = 1$, it is the threefold-degenerate $F_t = 1$ state which is lifted above the nondegenerate $F_t = 0$ state when considering only the yellow $J = 1/2$ states.

We want to perform a quick calculation to understand the behavior of the exchange interaction in a simplified model. This will allow us to investigate the impact of the correction terms, i.e., the band structure and central-cell corrections, by comparing our findings here with the results of the exact numerical calculation further below. Evaluating the integral for the matrix elements for the exchange interaction (12) with wave functions ψ_1 and ψ_2 over the δ term leads to a proportionality to $\psi_1^*(0)\psi_2(0)$. In a hydrogenlike model we choose the S states $\psi_1 = \psi_2 = \psi_{n,L=0,M=0}$. This yields

$$\langle n, L = 0, M = 0|H_{exch}|n, L = 0, M = 0\rangle = J_0\left(1 - \frac{1}{2\hbar^2}\boldsymbol{S}^2\right)V_{uc}\left(\frac{1}{\pi n a_B}\right)^3, \tag{13}$$

with the Bohr radius a_B. The relative energetic placement of multiplet states affected by the exchange interaction does not depend on the principal quantum number n in the hydrogenlike model, only the strength of the splitting, since n affects only an overall factor. As will be shown in Sec. III A, this does not hold in the case of the yellow excitons in cuprous oxide, where ortho- and paraexcitons are reversed for $n = 2$. For the other principal quantum numbers, the order of states is as shown in Fig. 1. Additionally, the splitting decreases with n^{-3} as a function of the principal quantum number in the simplified model. The situation is more complicated for the yellow exciton series in cuprous oxide, which will be more thoroughly discussed in Sec. III B.

B. Numerical diagonalization

To express the Schrödinger equation as a generalized eigenvalue problem, we use the complete basis introduced in Ref. [11]. In our basis states, the quasispin $\boldsymbol{I}$ and the hole spin $\boldsymbol{S}_h$ are coupled to form the effective hole spin $\boldsymbol{J}$. Near the Γ point, J is an approximate quantum number. Excitons with $J = 1/2$ and $J = 3/2$ belong to the yellow and green series, respectively. We further couple the effective hole spin $\boldsymbol{J}$ and the angular momentum $\boldsymbol{L}$ to $\boldsymbol{F}$, which is then coupled with the electron spin $\boldsymbol{S}_e$ to the total angular momentum $\boldsymbol{F}_t$. The quantization axis is chosen along the [001] direction of the crystal, and the corresponding z component of $\boldsymbol{F}_t$ is M_{F_t}. For the radial component we use the Coulomb-Sturmian functions [17], which are rescaled radial hydrogen atom solutions. The total basis states are thus given by

$$|\Pi\rangle = |N, L, (I, S_h)J, F, S_e, F_t, M_{F_t}\rangle. \tag{14}$$

The radial quantum number is defined as $N = n - L - 1$, with n being the principal quantum number. The resulting generalized eigenvalue problem is solved using a suitable LAPACK routine [18]. The material parameters used in our calculations are listed in Table I.

C. Experimental methods

In this section, we present the experimental methods used in this paper for the observation of the dark excitons in cuprous oxide. In short, the method presented in Ref. [23] was adjusted to optically activate the paraexcitons and to sensitively detect the resulting weak signals.

The paraexcitons are made allowed by applying a magnetic field, by which they gain an admixture of orthoexcitons through the associated symmetry reduction. Because the symmetry for particular rotations around the magnetic field is still maintained, the mixing occurs between states of the same symmetry class, which would be the same magnetic quantum number in the hydrogenlike model. As a result of this coupling, the involved states, typically forming a two-level system, repel each other. Since the coupling by the field is weak, the increase of the splitting between the states in the

TABLE I. Material parameters of Cu_2O used in the calculations.

Parameter	Value	Ref.
Energy gap	$E_g = 2.17208\,\text{eV}$	[1]
Spin-orbit coupling	$\Delta = 0.131\,\text{eV}$	[19]
Effective electron mass	$m_e = 0.99 m_0$	[20]
Effective hole mass	$m_h = 0.58 m_0$	[20]
Valence band parameters	$\gamma_1 = 1.76$	[19]
	$\gamma_2 = 0.7532$	[19]
	$\gamma_3 = -0.3668$	[19]
	$\eta_1 = -0.020$	[19]
	$\eta_2 = -0.0037$	[19]
	$\eta_3 = -0.0337$	[19]
Exchange interaction	$J_0 = 0.792\,\text{eV}$	[3]
Short distance correction	$V_0 = 0.539\,\text{eV}$	[3]
Lattice constant	$a = 0.42696\,\text{nm}$	[21]
Dielectric constants	$\varepsilon_{s1} = 7.5$	[22]
	$\varepsilon_{b1} = \varepsilon_{s2} = 7.11$	[22]
	$\varepsilon_{b2} = 6.46$	[22]
Energy of Γ_4^--LO phonons	$\hbar\omega_{LO1} = 18.7\,\text{meV}$	[15]
	$\hbar\omega_{LO2} = 87\,\text{meV}$	[15]

doublet can be well described by a quadratic dependence on the magnetic field.

Despite the hybridization of bright and dark states, the paraexciton oscillator strength remains small, so that efforts had to be made to distinguish the corresponding lines from orthoexciton states: In one-photon absorption the orthoexcitons with odd-symmetry envelopes, and, among them, mostly the *P* excitons, clearly dominate the spectra, including in the magnetic field. Therefore, we turned to two-photon excitation, detected subsequently by the coherent emission of photons at twice the frequency of the fundamental excitation laser, i.e., by second-harmonic generation.

For the SHG experiments, we use 200-fs laser pulses with a spectral width of 10 meV. The 6-mm-thick sample is cooled down to 1.4 K in superfluid helium. If allowed, the resulting spectra are typically dominated by orthoexcitons with even envelopes, but with much smaller oscillator strength compared to the *P* lines in one-photon absorption. This setting turned out to be sufficient to detect the paraexcitons if they are in energy sufficiently separated from orthostates.

For the excited paraexciton states this separation may be too small, so we also chose experimental configurations with respect to the crystal orientation relative to the light propagation as well as the polarization of the fundamental and second-harmonic light, for which the SHG signal does not appear at zero magnetic field and appears only due to the field application. Doing so facilitated carving out the weak paraexciton signals up to the principal quantum number $n = 6$. Further details of the experimental technique using optical second-harmonic generation and its instrumental implementation are given in Ref. [23].

III. RESULTS AND DISCUSSION

A. Reversal of yellow 2*S* ortho- and paraexcitons

In this section, we first briefly recapitulate the experimental observation of the positions of the yellow 2*S* ortho- and

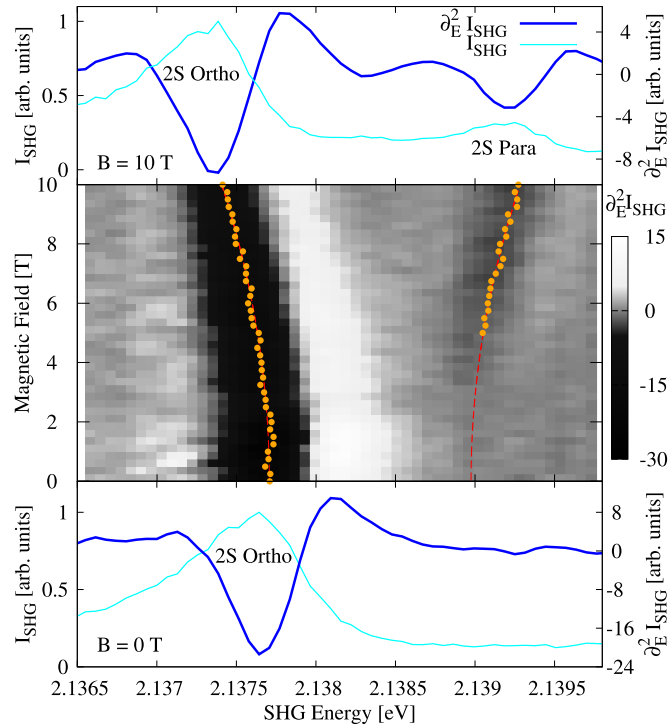

FIG. 2. Experimental SHG spectrum of the yellow 2*S* ortho- and paraexcitons. The wave vector $\boldsymbol{K}$ is parallel to the [111] axis, and the magnetic field is applied in Voigt geometry along the $[11\bar{2}]$ direction. The polarizations of the incoming and outgoing light are parallel to the magnetic field. We show a contour plot of the second derivative of the SHG intensity in gray scale. The positions of the ortho- and paraexcitons extracted by a Gaussian fit to the SHG intensity are marked with orange dots. Using a quadratic fit (red dashed line), we can extrapolate the energy of the paraexciton to $E_{B=0\,\text{T}}^{2S,\text{para}} = 2.13897\,\text{eV}$ at vanishing magnetic field. An analogous fit to the orthoexciton energies yields an energy $E_{B=0\,\text{T}}^{2S,\text{ortho}} = 2.13771\,\text{eV}$ at vanishing magnetic field. The top and bottom panels show the SHG intensity and its second derivative at magnetic field $B = 10\,\text{T}$ and $B = 0\,\text{T}$, respectively.

paraexcitons, presenting additional data not shown in Ref. [10]. Note that we assign the labels *green* and *yellow*, as well as the principal and angular quantum numbers in accordance with the assignments given in Ref. [3]. We then present the underlying mechanisms. Since the paraexciton is spin flip forbidden in electrical dipole and quadrupole transition experiments, we use a magnetic field to make them experimentally accessible. It is possible to include this magnetic field in the Hamiltonian introduced in Sec. II A (see, for example, Refs. [24–26]). In this work, we extrapolate the experimental values to vanishing magnetic field and analyze those in the numerical calculations. We therefore do not consider the magnetic field in the theory.

In the middle panel of Fig 2, we show a contour plot of the second derivatives of the SHG spectra of the 2*S* excitons. The corresponding SHG spectra measured at magnetic fields of 10 and 0 T are presented in the top and bottom panels, respectively. Spectra are measured with a spectral resolution of 80 μeV from 0 to 10 T in steps of 0.25 T in order to demonstrate the spectral shift of the 2*S* para- and orthoexcitons in a magnetic field. The wave vector is directed along the

SHG-allowed [111] axis, and the magnetic field is applied orthogonally to this in the $[11\bar{2}]$ direction. The polarization of the incoming and outgoing light is parallel to the magnetic field, i.e., $\boldsymbol{E}^{\text{in}} \parallel \boldsymbol{E}^{\text{out}} \parallel [11\bar{2}]$. This leads to a nonvanishing SHG signal of the paraexciton [27]. It is much weaker than the intensity of the orthoexciton and becomes only faintly visible at about 5 T. We therefore extrapolate the position of the paraexciton to zero magnetic field using a quadratic fit. We obtain $E^{2S,\text{para}}_{B=0\,\text{T}} = 2.13897\,\text{eV}$ for the paraexciton and $E^{2S,\text{ortho}}_{B=0\,\text{T}} = 2.13771\,\text{eV}$ for the orthoexciton. We can therefore experimentally confirm one of the curious features of the yellow paraexciton series in cuprous oxide predicted by Schweiner *et al.* [3], viz., the observation that the $2S$ paraexciton is located at a higher energy than the $2S$ orthoexciton. This shows that the experimentally observed behavior of the yellow excitons here is qualitatively different from the hydrogenlike model in this respect. Farenbruch *et al.* identified the origin of this reversal in the influence of the green $1S$ exciton [10]. In the following, we want to corroborate this with a detailed numerical analysis.

In Fig. 3(a) we show the exchange splitting for the yellow $2S$ state as a function of the parameter J_0, with the green states removed from the spectrum. For this calculation, we used only states with $J = 1/2$ in the basis. We see that in this case, the exchange interaction lifts the orthoexciton above the paraexciton as predicted. This confirms that the mixing with the $1S$ green orthoexciton is responsible for the surprising reversal because without the green state, the reversal is absent.

For a better understanding, we calculate the positions of the yellow $2S$ and green $1S$ states as a function of the spin-orbit coupling, revealing an avoided crossing. In Fig. 3(b) we show this avoided crossing between the yellow $2S$ and green $1S$ orthoexcitons. The green admixture of the states given by the expectation value

$$F_{J=3/2} = \langle \psi | P_{J=3/2} | \psi \rangle \tag{15}$$

of the projection operator onto the $J = 3/2$ Hilbert space for the exciton state ψ is indicated by the color bar. Using this green $J = 3/2$ fraction, we can identify the green states coming from the left-hand side and follow them through the crossing. This avoided crossing was already noted in Ref. [3], but the implications of the relative placement of the $2S$ para- and orthoexcitons were not discussed. We can see that the avoided crossing leads to the yellow $2S$ orthoexciton being placed below the $2S$ paraexciton for the actual value of the spin-orbit coupling $\Delta = 0.131\,\text{eV}$. For higher values at $\Delta \approx 0.15\,\text{eV}$, the ortho- and paraexcitons cross each other again, when the influence of the green Γ_5^+ $1S$ state is small enough. This further confirms and elucidates the influence of the mixing between the yellow and green series and its importance for a detailed understanding of the yellow excitons.

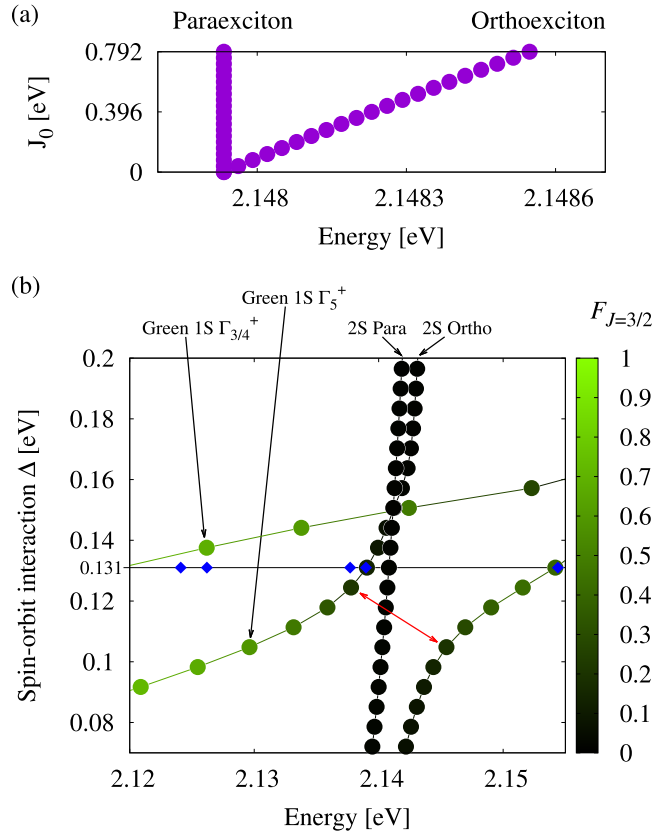

FIG. 3. (a) Splitting of the yellow $2S$ ortho- and paraexciton as a function of the strength of the exchange interaction J_0 when only the yellow $J = 1/2$ basis states are used for the diagonalization. In this case we observe that the orthoexciton is lifted above the paraexciton as expected. The exchange interaction is fully switched on for $J_0 = 0.792\,\text{eV}$ [3]. This shows that the exchange of the positions of the para- and orthoexciton has to originate in the influence of the green states. In (b), we show the responsible avoided crossing in the spectrum near the yellow $2S$ orthoexciton state as a function of the spin-orbit coupling Δ. We added lines to help guide the eyes. The green admixture $F_{J=3/2}$ to the states is indicated by the color bar. The horizontal line at $\Delta = 0.131\,\text{eV}$ marks the actual value of Δ in cuprous oxide. We can clearly see the avoided crossing between the yellow $2S$ orthoexciton and the Γ_5^+ green $1S$ state, marked in red. It is this avoided crossing that places the $2S$ orthoexciton below the $2S$ paraexciton. For larger values of Δ, the influence of the green $1S$ state diminishes, the $2S$ orthoexciton crosses the $2S$ paraexciton again, and the usual order between those states is reestablished. The experimental positions of the exciton states are marked by blue diamonds. We point out that the green Γ_3^+ and Γ_4^+ states are degenerate in our model calculations but show a small splitting in the experiment. This splitting is compatible with the cubic symmetry of the crystal, but the effect is not captured by our Hamiltonian.

B. Dependence of the exchange splitting on the principal quantum number

Since the removal of the mixing with the green $1S$ state restores the expected placement of ortho- and paraexcitons also in the case of the yellow $2S$ state, it is a natural question whether the exchange splitting decreases with the third power of the principal quantum number n^{-3} as in the hydrogenlike model, Eq. (13). In this section we want to investigate the exchange splitting of the yellow S excitons as a function of n. To remove the influence of the green $1S$ states, we use only the basis states with $J = 1/2$ belonging to the yellow series for the calculations here. In Fig. 4(a) we compare the numerical data for the full basis extracted from Table III in Ref. [3] with the exchange splitting if the influence of the green states is removed. We additionally show the actual experimental values for reference. A fit of the form $\Delta E_{\text{exch}}(n) = An^B$ reveals an

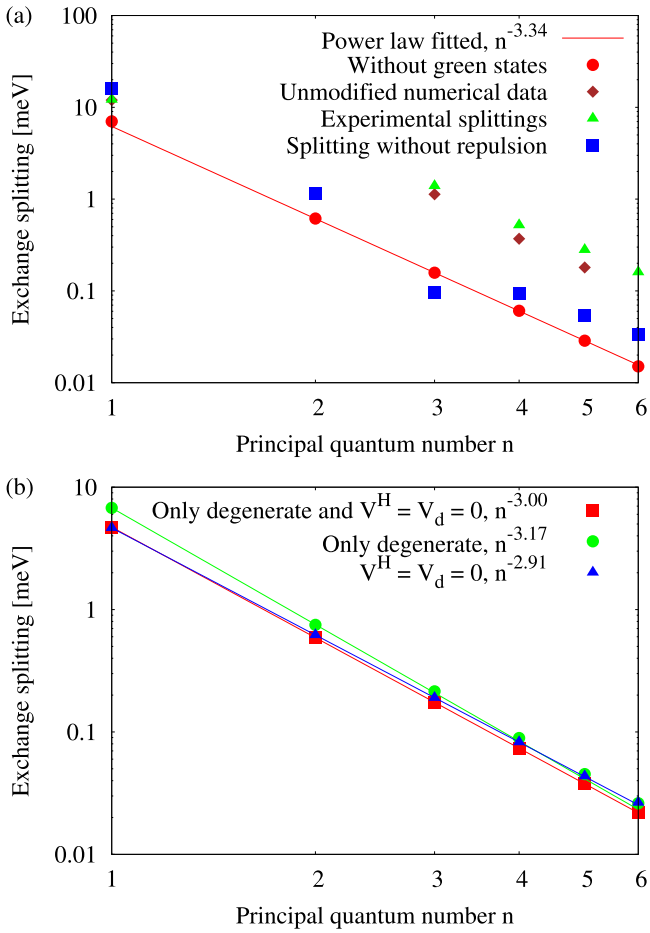

FIG. 4. Exchange splitting of the yellow excitons as a function of the principal quantum number n. To remove the influence of the green $1S$ exciton, only basis states with $J = 1/2$ were used. (a) Comparison of exchange splitting with (brown diamonds) and without (red circles) the influence of the green $1S$ state. Unmodified numerical data were taken from Ref. [3]. We additionally show the experimental values (green triangles) for reference. The blue squares show the splittings if the green state is included but the level repulsion between the green and yellow states due to the δ terms in the central-cell corrections is removed. (b) Exchange splitting as a function of n for modified material parameters, again with only the yellow $J = 1/2$ basis states. We show data for which we removed the influence of the Haken potential (blue triangles); data for which we diagonalized the exchange interaction only in the degenerate S spaces, neglecting the coupling between different principal quantum numbers (green circles); and data for which we combined the previous two conditions (red squares). The fits show that only the combination of all modifications leads to the decrease with the third power of the principal quantum number expected from the hydrogenlike model.

exponent $B = -3.34$ still differing from the expected $B = -3$ in the hydrogenlike model.

We identify two factors that explain this discrepancy. On the one hand, the Haken potential modifies the dielectric constant for small radii. This leads to a change in the effective Bohr radius and thus to a change in the value of the wave function at the origin. This disproportionally affects small quantum numbers and thus changes the dependency of the splitting on n. On the other hand, the exchange interaction is not diagonal in the principal quantum number; that is, the $2S$ state also influences the $1S$ state and so on. Going back to Eq. (12), we see that the matrix elements do not necessarily vanish if the principal quantum numbers of the coupled states differ. This also leads to a small but significant deviation from the n^{-3} behavior.

We illustrate the effects of the different factors in Fig. 4(b). We find that only if both of the factors discussed above are corrected for does the n^{-3} behavior from the hydrogenlike model emerge again.

Interestingly, the removal of the green $1S$ state also has a significant effect on the absolute size of the splitting between ortho- and paraexcitons in the range of principal quantum numbers shown, as can be seen in Fig. 4.

The most important effect accounting for this is the level repulsion caused by the exchange interaction and V_d matrix elements between the green orthoexciton and the yellow Γ_5^+ states. The green Γ_5^+ exciton repels the yellow Γ_5^+ states, but the green Γ_4^+ and Γ_3^+ states leave the yellow paraexcitons of symmetry Γ_2^+ unaffected. For yellow states energetically higher than the green $1S$ state, this increases the splitting, whereas for those that are lower, it decreases it. The blue squares in Fig. 4(a) show the splittings of the yellow excitons when this repulsion is removed. The resulting splittings in the yellow exciton series are far smaller than the experimental values for $n \geqslant 4$ and more in line with the values when the green $1S$ state is removed completely, as can be seen by comparison with the red circles. For the yellow $1S$ state, the effect is reversed, and the removal of the level repulsion increases the splitting instead.

C. Splitting of yellow 1S state vs green 1S state

In this section we investigate the difference in the strength between the exchange splitting of the green $1S$ state compared to the yellow $1S$ state. We want to explain why the splitting of the green states is more than double that of the yellow states.

Diagonalizing the yellow series alone without the green $J = 3/2$ basis states, we find that the splitting of the yellow $1S$ excitons is approximately 7.02 meV, which is even smaller than the value with the full basis. Diagonalizing the green states alone, the splitting of the green $1S$ excitons is approximately 27.07 meV. The discrepancy cannot, therefore, be explained by the mutual level shifts between the green $1S$ state and the yellow spectrum.

We again find that there are two factors which actually explain this difference. The first factor is the fact that the eigenvalues of the operator $\boldsymbol{S}_\mathrm{e} \cdot \boldsymbol{S}_\mathrm{h}$ differ between the $J = 1/2$ and $J = 3/2$ Hilbert spaces. According to the Appendix of Ref. [3], the matrix elements in the basis (14) are given by

$$\begin{aligned} M &= \langle \Pi' | \boldsymbol{S}_\mathrm{e} \cdot \boldsymbol{S}_\mathrm{h}\, \delta(\boldsymbol{r}) | \Pi \rangle \\ &= \delta_{L'0}\delta_{L0}\delta_{F_\mathrm{t}F_\mathrm{t}'}\delta_{M_{F_\mathrm{t}}M_{F_\mathrm{t}}'}\, \frac{3}{2\pi}(-1)^{F_\mathrm{t}+F'+F+J+J'} \\ &\quad \times [(2F+1)(2F'+1)(2J+1)(2J'+1)]^{\frac{1}{2}} \\ &\quad \times \begin{Bmatrix} F' & F & 1 \\ \frac{1}{2} & \frac{1}{2} & F_\mathrm{t} \end{Bmatrix} \begin{Bmatrix} F & F' & 1 \\ J' & J & 0 \end{Bmatrix} \begin{Bmatrix} \frac{1}{2} & J' & 1 \\ J & \frac{1}{2} & 1 \end{Bmatrix}. \end{aligned} \tag{16}$$

TABLE II. Energies of the lowest yellow and green 1S excitons for different choices of the parameters in the central-cell corrections with the exchange interaction removed. For the yellow values, we diagonalized only the $J = 1/2$ Hilbert space, and for the green values we diagonalized only the $J = 3/2$ Hilbert space. For the gap energies we used $E_{\mathrm{gap,yellow}} = 2.17208\,\mathrm{eV}$ and $E_{\mathrm{gap,green}} = 2.30308\,\mathrm{eV}$.

Series	V_d	V^{H}	E_{1S} (eV)	E_{Ryd} (meV)
Yellow	on	on	2.059	112.8
Yellow	on	off	2.076	95.9
Yellow	off	off	2.086	86.1
Green	on	on	2.153	150.5
Green	on	off	2.179	124.1
Green	off	off	2.198	105.3

Fixing either $J = J' = 1/2$ or $J = J' = 3/2$, the operator is already diagonal in the given basis. We can evaluate the matrix elements for the yellow and green series and $L = L' = 0$. For $J = J' = 1/2$, we calculate $M = 1/4\pi$ with $F_{\mathrm{t}} = 0$ and $M = -1/12\pi$ with $F_{\mathrm{t}} = 1$. For $J = J' = 3/2$ it is $M = 1/4\pi$ when $F_{\mathrm{t}} = 2$ and $M = -5/12\pi$ when $F_{\mathrm{t}} = 1$. Note that the exchange interaction (12) contains this operator with reversed sign. The exchange interaction therefore lifts the $F_{\mathrm{t}} = 1$ states above the others in both the yellow and green series, as depicted in Fig. 1. We thus find that the splitting in the eigenvalues for $J = 3/2$ is $\Delta M_{\mathrm{green}} = 2/3\pi$ and, consequently, exactly double the splitting for $J = 1/2$, which is $\Delta M_{\mathrm{yellow}} = 1/3\pi$.

These calculations account for part of the difference between the yellow and green splittings. A factor of approximately 1.93 between the green and yellow splittings remains to be explained. Because of the δ term, the exchange splitting is proportional to $|\psi(0)|^2$, which in turn is proportional to the inverse third power of the Bohr radius a_{B}^{-3}. Since the Bohr radius is proportional to the reduced mass μ, it follows that $|\psi(0)|^2 \sim \mu^3$. This seems to be the explanation for the factor of 1.93, as explained in the following. The reduced mass is proportional to the Rydberg energy in a hydrogenlike system. To approximate the latter, we calculated the binding energy of the yellow and green 1S states while varying the exact form of the potential. The results are listed in Table II. Based on these data, we can estimate the ratio of the reduced masses of the green and yellow 1S states with the ratio of the binding energies. Since the latter are not only affected by the Coulomb interaction but also by the additional terms V^{H} and V_d in Eq. (7), we need to correct for those. Using the values where the central-cell corrections are removed completely, we get

$$\left(\frac{\mu_{\mathrm{green}}}{\mu_{\mathrm{yellow}}}\right)^3 \approx \left(\frac{E_{\mathrm{Ryd}}^{\mathrm{green}}}{E_{\mathrm{Ryd}}^{\mathrm{yellow}}}\right)^3 \approx \left(\frac{105.3\,\mathrm{meV}}{86.1\,\mathrm{meV}}\right)^3 \approx 1.22^3 \approx 1.82. \tag{17}$$

This is in good agreement with the factor of 1.93. The explanation for the different strengths of the exchange splitting in the yellow and green 1S exciton states therefore is, on the one hand, the factor of 2 due to the operator $\boldsymbol{S}_{\mathrm{e}} \cdot \boldsymbol{S}_{\mathrm{h}}$ for $J = 1/2$ and $J = 3/2$ and, on the other hand, the difference in the reduced mass μ for the yellow and green 1S excitons.

IV. SUMMARY AND CONCLUSION

Experimental investigations into the paraexciton series of yellow excitons in Cu_2O and corresponding exchange splittings revealed a number of ways in which a simple hydrogenlike model is insufficient. In this paper, we numerically investigated spectra with modified material parameters and thus gained experimentally inaccessibly insights. We used this to interpret the experimental findings in Ref. [10] and identify their roots in the properties of the system.

We first investigated the reversal of the yellow 2S para- and orthoexcitons. Farenbruch *et al.* [10] identified the mixture with the 1S green orthoexciton as the origin of the reversal. We were able to corroborate this explanation with detailed calculations. We showed that the orthoexciton is lifted above the paraexciton if the influence of the green excitons is removed in the simulation. Varying the spin-orbit coupling revealed an avoided crossing between the yellow 2S orthoexciton and the green 1S exciton which explains the placement of the orthoexciton below the paraexciton. We were thus able to show how the coupling of the yellow and green series leads to a behavior that qualitatively differs from the hydrogenlike approximation, underscoring its importance for the understanding of the yellow exciton series.

Removing the influence of the green states, the expected order of states is restored. In this case, does the exchange splitting decrease with the third power of the principal quantum number n? Our calculations show that this is not exactly the case. We identify two reasons for this. First of all, the Haken potential changes the dielectric constant for small radii, which influences the wave function at the origin and therefore the splitting. A simplified treatment of the exchange splitting also overlooks the second factor, which is the coupling between S states of different principal quantum numbers by the exchange splitting itself. A systematic analysis shows that these two factors account for the discrepancy from the n^{-3} behavior.

We concluded by studying the origin of the large difference between the exchange splittings of the yellow and green 1S states. Farenbruch *et al.* [10] confirmed the prediction by Schweiner *et al.* [3] that the splitting of the green 1S exciton is over 30 meV and therefore about 2.5 times the splitting of about 12 meV for the yellow 1S state. We also identified two reasons to account for this. The first is the difference in the matrix elements of $\boldsymbol{S}_{\mathrm{e}} \cdot \boldsymbol{S}_{\mathrm{h}} \delta(\boldsymbol{r})$ for $J = 1/2$ and $J = 3/2$. Since the exchange splitting depends upon the relative orientation of the electron and hole spins, different values of the effective hole spin $\boldsymbol{J} = \boldsymbol{I} + \boldsymbol{S}_{\mathrm{h}}$ lead to different strengths of the exchange splitting. The second is the difference in the reduced masses between the yellow and green 1S states. The reduced mass of the green 1S state is significantly higher than the reduced mass of the yellow 1S state, as revealed by a detailed analysis of the Rydberg energy when correcting for the influence of short-distance terms in the Hamiltonian. This leads to a higher value of the wave function at the origin and a corresponding increase of the exchange splitting.

ACKNOWLEDGMENTS

The theoretical studies at the University of Stuttgart were supported by Deutsche Forschungsgemeinschaft (Grant

No. MA1639/13-1). The experimental studies at the TU Dortmund were supported by the Deutsche Forschungsgemeinschaft through the International Collaborative Research Centre TRR 160 (Projects No. A8 and No. C8). We also acknowledge the support from Project No. AS 459/1-3. We thank F. Schweiner for his contributions.

[1] T. Kazimierczuk, D. Fröhlich, S. Scheel, H. Stolz, and M. Bayer, Giant Rydberg excitons in the copper oxide Cu_2O, Nature (London) **514**, 343 (2014).

[2] M. Aßmann, J. Thewes, D. Fröhlich, and M. Bayer, Quantum chaos and breaking of all anti-unitary symmetries in Rydberg excitons, Nat. Mater. **15**, 741 (2016).

[3] F. Schweiner, J. Main, G. Wunner, and Ch. Uihlein, Even exciton series in Cu_2O, Phys. Rev. B **95**, 195201 (2017).

[4] E. Poem, Y. Kodriano, C. Tradonsky, N. H. Lindner, B. D. Gerardot, P. M. Petroff, and D. Gershoni, Accessing the dark exciton with light, Nat. Phys. **6**, 993 (2010).

[5] D. Snoke and G. M. Kavoulakis, Bose–Einstein condensation of excitons in Cu_2O: Progress over 30 years, Rep. Prog. Phys. **77**, 116501 (2014).

[6] M. Beian, M. Alloing, R. Anankine, E. Cambril, C. Gomez Carbonell, A. Lemaître, and F. Dubin, Spectroscopic signatures for the dark Bose-Einstein condensation of spatially indirect excitons, Europhys. Lett. **119**, 37004 (2017).

[7] G. Kuwabara, M. Tanaka, and H. Fukutani, Optical absorption due to paraexciton of Cu_2O, Solid State Commun. **21**, 599 (1977).

[8] J. Brandt, D. Fröhlich, C. Sandfort, M. Bayer, H. Stolz, and N. Naka, Ultranarrow Optical Absorption and Two-Phonon Excitation Spectroscopy of Cu_2O Paraexcitons in a High Magnetic Field, Phys. Rev. Lett. **99**, 217403 (2007).

[9] A. Mysyrowicz, D. P. Trauernicht, J. P. Wolfe, and H. R. Trebin, Stress dependence of the paraexciton in Cu_2O, Phys. Rev. B **27**, 2562 (1983).

[10] A. Farenbruch, D. Fröhlich, D. R. Yakovlev, and M. Bayer, Rydberg Series of Dark Excitons in Cu_2O, Phys. Rev. Lett. **125**, 207402 (2020).

[11] F. Schweiner, J. Main, M. Feldmaier, G. Wunner, and Ch. Uihlein, Impact of the valence band structure of Cu_2O on excitonic spectra, Phys. Rev. B **93**, 195203 (2016).

[12] R. S. Knox, *Theory of Excitons* (Academic, New York, 1963).

[13] Ch. Uihlein, D. Fröhlich, and R. Kenklies, Investigation of exciton fine structure in Cu_2O, Phys. Rev. B **23**, 2731 (1981).

[14] D. Fröhlich, R. Kenklies, Ch. Uihlein, and C. Schwab, Assignment of the Even-Parity Excitons in Cu_2O, Phys. Rev. Lett. **43**, 1260 (1979).

[15] G. M. Kavoulakis, Y. C. Chang, and G. Baym, Fine structure of excitons in Cu_2O, Phys. Rev. B **55**, 7593 (1997).

[16] P. Schmelcher and L. S. Cederbaum, Regularity and chaos in the center of mass motion of the hydrogen atom in a magnetic field, Z. Phys. D **24**, 311 (1992).

[17] M. A. Caprio, P. Maris, and J. P. Vary, Coulomb-Sturmian basis for the nuclear many-body problem, Phys. Rev. C **86**, 034312 (2012).

[18] E. Anderson, Z. Bai, C. Bischof, S. Blackford, J. Demmel, J. Dongarra, J. D. Croz, A. Greenbaum, S. Hammarling, and A. McKenney, *LAPACK Users' Guide*, 3rd ed. (Society for Industrial and Applied Mathematics, Philadelphia, 1999).

[19] F. Schöne, S.-O. Krüger, P. Grünwald, H. Stolz, S. Scheel, M. Aßmann, J. Heckötter, J. Thewes, D. Fröhlich, and M. Bayer, Deviations of the exciton level spectrum in Cu_2O from the hydrogen series, Phys. Rev. B **93**, 075203 (2016).

[20] J. W. Hodby, T. E. Jenkins, C. Schwab, H. Tamura, and D. Trivich, Cyclotron resonance of electrons and of holes in cuprous oxide, Cu_2O, J. Phys. C **9**, 1429 (1976).

[21] H. E. Swanson and R. K. Fuyat, Standard X-ray diffraction powder patterns, Natl. Bur. Stand. Circ. (U. S.) 539 **II**, 23 (1953).

[22] O. Madelung, U. Rössler, and M. Schulz, eds., *Landolt-Börnstein - Group III Condensed Matter* (Springer, Berlin, 1998).

[23] A. Farenbruch, J. Mund, D. Fröhlich, D. R. Yakovlev, M. Bayer, M. A. Semina, and M. M. Glazov, Magneto-Stark and Zeeman effect as origin of second harmonic generation of excitons in Cu_2O, Phys. Rev. B **101**, 115201 (2020).

[24] F. Schweiner, J. Main, G. Wunner, M. Freitag, J. Heckötter, Ch. Uihlein, M. Aßmann, D. Fröhlich, and M. Bayer, Magnetoexcitons in cuprous oxide, Phys. Rev. B **95**, 035202 (2017).

[25] P. Rommel, F. Schweiner, J. Main, J. Heckötter, M. Freitag, D. Fröhlich, K. Lehninger, M. Aßmann, and M. Bayer, Magneto-Stark effect of yellow excitons in cuprous oxide, Phys. Rev. B **98**, 085206 (2018).

[26] P. Rommel, J. Main, A. Farenbruch, J. Mund, D. Fröhlich, D. R. Yakovlev, M. Bayer, and Ch. Uihlein, Second harmonic generation of cuprous oxide in magnetic fields, Phys. Rev. B **101**, 115202 (2020).

[27] A. Farenbruch, D. Fröhlich, D. R. Yakovlev, and M. Bayer, Two-photon absorption and second harmonic generation of 1*S* para- and orthoexcitons in Cu_2O coupled by a magnetic field, Phys. Rev. B **102**, 115203 (2020).